Analysis of downlink transmission in DCO-OFDM-based optical attocell networks

Analysis of Downlink Transmission in DCO-OFDM-Based Optical Attocell Networks

Cheng Chen, Muhammad Ijaz, Dobroslav Tsonev and Harald Haas
Institute for Digital Communications
Li-Fi R&D Centre
The University of Edinburgh EH9 3JL, Edinburgh, UK
{cheng.chen, m.ijaz, d.tsonev, h.haas}@ed.ac.uk

***Abstract*—In this paper, an indoor visible light communication (VLC) cellular network, referred to as an optical attocell network, is analysed at system level. A line-of-sight (LOS) ray-tracing model is used to characterise the light propagation and its effect on the performance of an intensity modulation (IM) and direct detection (DD) communication system. Orthogonal frequency division multiple access (OFDMA) based on direct-current optical orthogonal frequency division multiplexing (DCO-OFDM) is used as a multi-user access scheme. The signal-to-interference-plus-noise ratio (SINR) for a user with a random location in an optical attocell is studied. An analytical approach to calculate the statistics of the SINR is presented and verified by Monte Carlo simulations. Moreover, average spectral efficiency is also studied in order to estimate the downlink wireless capacity of the optical attocell network. The spectral efficiency of the system has been found to be strongly dependent on the radius of an optical attocell and on the half-power semi-angle of the light transmission profile. Guidelines for the configuration of the relevant attocell parameters are provided. An optical attocell with an average spectral efficiency of 5.9 bits/s/Hz is demonstrated for an appropriate set of attocell parameters.**

***Index Terms*—visible light communications, cellular networks, optical orthogonal frequency division multiplexing and orthogonal frequency division multiple access.**

I. Introduction

The shortage of spectral resources in the radio frequency (RF) region has sparked considerable research interest in the field of optical wireless communications (OWC) for indoor applications [1]. In particular, a lot of interest has been directed towards the visible light spectrum. VLC can offer data transmission and lighting functionality concurrently. A VLC system can be realised with a light emitting diode (LED) as a transmitter and a photodiode (PD) as a detector. Due to the incoherent emission of the LED, coherent modulation/detection techniques are not possible in VLC. Therefore, intensity modulation with direct detection techniques have to be used to encode data. VLC offers several advantages over RF communication systems [2]. For example, a VLC system generates virtually no electromagnetic radiation in the RF spectrum region. Additionally, VLC is inherently robust against eavesdropping. Furthermore, due to the intrinsic properties of light there is no co-channel interference (CCI) between VLC systems in adjacent rooms, which indicates that the optical spectral resources can be reused aggressively in space.

It is widely recognised that an increased spatial reuse of spectral resources offers a considerable gain in wireless capacity [3]. VLC offers a unique opportunity to create a small-scale cellular network that can be embedded into a room with multiple light fixtures, thereby further reducing the reuse distance of the optical spectral resource. In this type of cellular networks, each spatially separated lighting element is used as a base station (BS), which covers multiple users in the small area (typically 1-10 m^2) underneath it. A system of this kind offers full coverage to users in an indoor environment. It is also expected to provide a considerable improvement in wireless system capacity compare to RF communication. Optical orthogonal frequency division multiplexing (O-OFDM) has been researched as one of the prime candidates for signal modulation in VLC [4], [5]. It provides an optimal utilization of the communication resources through adaptive modulation and coding (AMC). Moreover, O-OFDM offers a straightforward multi-user access scheme which is referred to as: OFDMA. Since the DC-bias in DCO-OFDM is harnessed for illumination purposes [6], DCO-OFDM can be used to achieve a high spectral efficiency in the downlink transmission. When illumination is not required such as in the uplink, an power and spectral efficient OFDM variant named enhanced unipolar OFDM [7] can be used.

A number of studies on optical wireless networks have been carried out. The authors of [8] have proposed a cellular scheme to mitigate CCI using a larger spatial reuse distance in an indoor infrared wireless communication system. In [9], the performance of optical wireless hotspots was compared to that achieved by an RF system. That study also investigated the relationship between signal-to-noise ratio (SNR) and the horizontal distance of a user from the cell centre. A VLC system adopting cellular characteristics using a light shaping diffuser was proposed in [10]. A small-cell optical cellular network with full function of an RF cellular system has been proposed in [6]. In an RF cellular system, a personal femtocell is known as an attocell [11]. In [6], the optical small-cell network is referred to as an optical attocell network. However, unlike the personal RF attocell, the light properties and the existing infrastructure readily allow for full wireless indoor networking, but with cell sizes much smaller than that used in heterogeneous RF wireless networks. An optical attocell

978-1-4799-3512-3/14/$31.00 ©2014 IEEE

network is characterised by multiple optical access points (APs) where one AP serves multiple users, and multiple users can communicate to one or more optical APs in the uplink. In addition, it also allows for user mobility and enables handover.

In this paper, a system level analysis of the downlink transmission in an optical attocell network based on DCO-OFDM is proposed. The SINR for a user and system average spectral efficiency are considered and investigated. Analytical method to calculate the cumulative distribution function (CDF) of the SINR and for the average spectral efficiency are provided and validated by Monte Carlo simulation. The impact of important parameters such as the radius of an optical attocell and the half-power semi-angle of the light emission profile is also studied.

The remainder of the paper is organized as follows: Section II presents the system model of the considered optical attocell network. Section III presents the analysis of the SINR. Section IV presents the analysis of the average spectral efficiency. Finally, conclusions are presented in Section V.

II. System Model

The downlink geometric deployment in an optical attocell network is illustrated in Fig. 1. The following assumptions are made in order to simplify the analysis: i) BSs are placed in a regular hexagonal lattice, since this deployment minimises the overlap between coverage areas of adjacent BSs; ii) the ceiling luminaries (BS downlink transmitters) are considered as point sources and are facing downward; iii) each user has a downlink receiver with a PD facing straight up; iv) the concentrator and optical filter are assumed to have unity gain; v) the vertical separation between a BS and a user is fixed with a specified distance h; vi) the receiver field of view (FOV) is wide enough for the users in a given cell to receive the signal from the tagged BS and from the BSs in the six neighbouring cells only. This FOV configuration guarantees a seamless coverage of the system with a minimum number of interference sources.

A. Propagation Model

The reflection paths are omitted in this study for a number of reasons. First of all, the optical OFDM techniques are adopted. One of the motivations for using OFDM is that it is more resilient to inter-symbol interference (ISI) with low complexity equalisation in the frequency domain. Secondly, a deployment in a large indoor environment with sparse reflection objects (e.g. walls, furnitures) is assumed in this study, which has a less dispersive channel power delay profile in the major part of the room. In addition, a commercially available white LED is assumed to be used in the considered system. A typical white LED has a 3 dB bandwidth of about 20 MHz when combined with a blue filter at the receiver side [12]. This means that the sample period is long enough to have the signal power from the LOS path and the short reflected paths (at most 15 m longer than the LOS path) fall into a single symbol time slot. On the other hand, the ISI power caused by the rest of the reflection paths is negligible (more than 30 dB smaller compared to the LOS signal power). Therefore, only the LOS path is considered in the light propagation for the downlink transmission. In other words, the users generally experience a communication channel with a near-flat frequency response. As shown in [13], the LOS optical channel can be well-characterised by its direct-current (DC) gain. The DC gain of the channel from BS_i to an given user is given as:

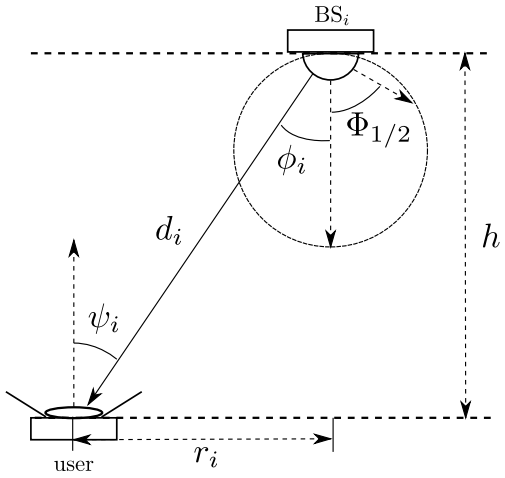

Fig. 1. Downlink system link in an optical attocell network.

$$G_i = \frac{(m+1)A_{\mathrm{pd}}}{2\pi d_i^2}\cos^m(\phi_i)\cos(\psi_i), \tag{1}$$

where m denotes the Lambertian emission order, which is given by $m = -\ln(2)/\ln(\cos(\Phi_{1/2}))$ where $\Phi_{1/2}$ is the half-power semi-angle of the LED; A_{pd} is the physical area of the user receiver PD; d_i represents the Euclidean distance between BS_i and the user; ϕ_i denotes the corresponding light radiance angle; and ψ_i is the light incidence angle, in which $i = 0, 1, 2, \cdots$. BS_0 corresponds to the tagged BS, while the rest of the BSs are interfering BSs.

B. Orthogonal Frequency Division Multiple Access

The application of DCO-OFDM can be extended to an OFDMA system to realise multi-user access in an optical attocell network. The K frequency domain quadrature amplitude modulated data symbols before the inverse discrete Fourier transform (IDFT) are defined as $\boldsymbol{X} = [X_0\, X_1\, X_2\, \cdots\, X_{K-1}]$. Since an intensity modulated signal is a real-valued signal, Hermitian symmetry is required to make the OFDM symbols contain only real samples. This requires that $X_k = X_{K-k}^*$, where $[\cdot]^*$ is the complex conjugate operation. In addition, X_0 and $X_{K/2}$ are set to zero [5]. Consequently, only $K_{\mathrm{t}} = K/2 - 1$ symbols carry information. Through the K-point IDFT and the addition of a DC-bias, the time domain OFDM symbol can be described as follows:

$$\boldsymbol{x}(t) = x_{\mathrm{DC}} + \sum_{k=0}^{K-1} \boldsymbol{x}_k(t),\ t = 0, 1, \cdots, K-1, \tag{2}$$

$$\boldsymbol{x}_k(t) = \frac{\boldsymbol{X}(k)}{\sqrt{K}}\exp\left(\frac{2\pi jkt}{K}\right), \tag{3}$$

where x_{DC} is the DC-bias and $\boldsymbol{x}_k(t)$ represents the signal component at time t which accounts for the modulated symbol on subcarrier k. After the addition of a DC-bias, any remaining negative samples are set to zero. Since the required cyclic-prefix (CP) length is typically short in OWC [14], the effect of adding a CP is omitted in this study. In a multiple access version of DCO-OFDM, the K_{t} transmission channels are shared by a number of users. Each user is allocated one or more subcarriers for transmission. Assuming perfect sampling and synchronization, the sample received at time t of the intensity modulated signal received by an given user on subcarrier k can be expressed as:

$$\boldsymbol{y}_k(t) = \boldsymbol{x}_{0,k}(t)G_0R_{\mathrm{pd}} + \sum_{i\in И} \boldsymbol{x}_{i,k}(t)G_iR_{\mathrm{pd}} + \boldsymbol{n_k}(t), \quad (4)$$

where $\boldsymbol{x}_{i,k}(t)$ is the transmitted signal from BS_i on subcarrier k at time t; In the case of $i = 0$, $\boldsymbol{x}_{0,k}(t)$ is the desired transmitted signal for the given user; R_{pd} denotes the responsivity of the PD; and $\boldsymbol{n_k}(t)$ represents the user receiver noise signal on subcarrier k. The noise is dominated by shot noise and thermal noise with a noise power spectral density (PSD) of N_0. Therefore, $\boldsymbol{n_k}$ has zero mean and a variance of $\sigma_k^2 = N_0W_{\mathrm{sc}}$, where W_{sc} is the bandwidth of each subcarrier. Assuming a total intensity modulation bandwidth of W, W_{sc} can be expressed as $W_{\mathrm{sc}} = W/K$. The second term of $\boldsymbol{y}_k$ accounts for the received interference signal, where $И$ is the set of all of the interfering BSs. Because the channel has a near-flat frequency response, the maganitude response over the whole frequency band is assumed to be unity. Clipping noise and non-linearities of the LED are not considered as these are outside the scope of this study.

III. Signal-to-Interference-Plus-Noise Ratio Assessment

A. SINR model Setup

SINR is an important metric to measure the quality of a wireless connection. Similar to the definition of SNR in an IM/DD OWC system, SINR is defined as the ratio of the received desired signal electrical power to the noise and interference electrical power. Based on (4), the SINR for the given user on subcarrier k is given as:

$$\gamma_k = \frac{P_{\mathrm{elec},0,k}G_0^2R_{\mathrm{pd}}^2}{\sum\limits_{i\in И} P_{\mathrm{elec},i,k}G_i^2R_{\mathrm{pd}}^2 + \sigma_k^2}, \quad (5)$$

where $P_{\mathrm{elec},i,k}$ denotes the electrical signal power transmitted by BS_i on subcarrier k. The conversion between the average electrical power and the average optical power obeys the following relationship in a DCO-OFDM system as [15]:

$$\frac{P_{\mathrm{opt}}^2}{P_{\mathrm{elec,AC}} + x_{\mathrm{DC}}^2} = \frac{\kappa^2}{1+\kappa^2}, \quad (6)$$

$$\kappa = x_{\mathrm{DC}}/\sqrt{P_{\mathrm{elec,AC}}}, \quad (7)$$

where $P_{\mathrm{opt}} = \mathbb{E}[\boldsymbol{x}(t)] = x_{\mathrm{DC}}$ is the average transmitted optical power in which $\mathbb{E}[\cdot]$ is the expectation operator, and $P_{\mathrm{elec,AC}} = \mathbb{E}[\sum_{k=0}^{K-1} \boldsymbol{x}_k^2(t)] = \sum_{k=0}^{K-1} \mathbb{E}[\boldsymbol{x}_k^2(t)]$ denotes the total electrical power for transmission excluding the DC-bias. After rearranging (6), it can be found that:

$$P_{\mathrm{elec,AC}} = P_{\mathrm{opt}}^2/\kappa^2. \quad (8)$$

It is assumed that an equal power allocation is conducted over the $K-2$ subcarriers that carry signals, and all BS transmitters emit the same average optical power. Then:

$$P_{\mathrm{elec},i,k} = \frac{P_{\mathrm{opt}}^2}{(K-2)\kappa^2}. \quad (9)$$

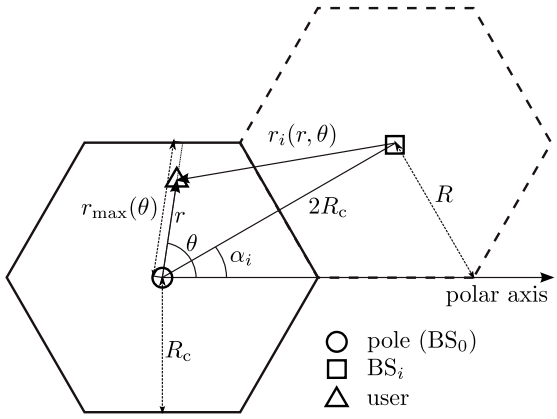

Fig. 2. Optical attocell network geometry model with a polar coordinate system.

B. SINR Statistics Analysis

In this subsection, we conduct an analysis of the statistics of the SINR based on the randomness of the user locations. It is assumed that the user location follows a uniform distribution in an optical attocell. The objective is to find the CDF of the SINR for a user. However, there are a number of variables present in (1) which are related to user location. In order to simplify the analysis, the following modification in (1) is carried out. From Fig. 1, it can be found that:

$$\cos(\phi_i) = \cos(\psi_i) = \frac{h}{d_i}, \quad (10)$$

$$d_i = \sqrt{r_i^2 + h^2}, \quad (11)$$

where r_i is the horizontal separation between BS_i and the user. Inserting (10) and (11) into (1) gives:

$$G_i = \frac{(m+1)A_{\mathrm{pd}}h^{m+1}}{2\pi}(r_i^2+h^2)^{-\frac{m+3}{2}}. \quad (12)$$

With this step, the number of variables in the light propagation model is reduced to one. By inserting (12) into (5) and by rearranging, (5) can be rewritten as:

$$\gamma_k = \frac{(r_0^2+h^2)^{-m-3}}{\sum\limits_{i\in И}(r_i^2+h^2)^{-m-3} + \Omega}, \quad (13)$$

where

$$\Omega = \frac{4\pi^2\kappa^2N_0W(K-2)}{\left((m+1)A_{\mathrm{pd}}h^{m+1}P_{\mathrm{opt}}R_{\mathrm{pd}}\right)^2K}. \quad (14)$$

TABLE I
SYSTEM PARAMETERS

Parameter	Symbol	Value
BS LED optical power	P_{opt}	10 W
vertical separation	h	2.15 m
Noise PSD	N_0	1×10^{-21} A^2/Hz
PD area	A_{pd}	1 cm^2
PD responsivity	R_{pd}	0.6 A/W
DC bias factor	κ	3

Since the observed optical attocell coverage area is rotational symmetric, it is reasonable to determine the user location with a polar coordinate system as shown in Fig. 2. The pole of the coordinate is defined at the centre of the tagged cell. The direction of the polar axis is shown in Fig. 2. The location of a user is defined by two variables r and θ. The variable r denotes the horizontal separation between user and the pole. The variable θ represents the polar angle corresponding to the user location. The location of a user in an optical attocell is confined within a hexagon. Therefore, for a user with a specified θ, the possible r should be within a in a specified region. The smallest r is intuitively zero, while the maximum possible r can be calculated as a function of θ as:

$$r_{\max}(\theta) = R_{\text{c}} / \cos\left(\theta \bmod \frac{\pi}{3} - \frac{\pi}{6}\right), \tag{15}$$

where R_{c} is defined as the distance between the pole and an edge of the optical attocell. The radius of the the cell is denoted by R, which is defined as the distance between the pole and a vertex of the cell boundary. The variables R_{c} and R satisfy the following relationship: $R_{\text{c}} = \sqrt{3}R/2$, see Fig. 2.

Furthermore, r_i in (13) can be calculated from the user location variables r and θ. Since the tagged BS is just located at the pole of the coordinate, r_0 equals r. According to the hexagonal layout of the BSs, we can find that BS$_i$ is located at $(2R_{\text{c}}, \alpha_i)$, where

$$\alpha_i = \frac{\pi i}{3} - \frac{\pi}{6}, i = 1, 2, \ldots, 6. \tag{16}$$

By considering the triangle with vertices at the pole, the given user and the BS$_i$, it can be shown that r, θ and r_i are related to each other by the law of cosines as demonstrated in Fig. 2. Therefore, r_i can be calculated with the following expression:

$$r_i(r, \theta) = \sqrt{r^2 - 4R_{\text{c}} r \cos(\theta - \alpha_i) + 4R_{\text{c}}^2}. \tag{17}$$

By applying the above variable substitution, (13) can be modified to a function of the user location (r, θ) as:

$$\gamma(r, \theta) = \frac{(r^2 + h^2)^{-m-3}}{\sum_{i=1}^{6} (r_i(r, \theta)^2 + h^2)^{-m-3} + \Omega}. \tag{18}$$

In order to find the distribution of $\gamma(r, \theta)$, the statistics of r and θ should be known. The determination of the distribution of r and θ can be fomulated as a problem in geometric probability. This can be solved by evaluating the volume ratio [16]. For example, a point is uniformly distributed within a given set Ш. Set Д is defined as a subset of Ш. Then the probability that the point falls in Д can be calculated as the ratio of the volume of Д to the volume of Ш. Following this approach, the conditional probability density function (PDF) of r with a specified θ and the PDF of θ can be calculated as follows:

$$f_r(r|\theta) = \frac{2r}{r_{\max}^2(\theta)}, \tag{19}$$

$$f_\theta(\theta) = \frac{r_{\max}^2(\theta)}{4\sqrt{3}R_{\text{c}}^2}. \tag{20}$$

The conditional PDF of the SINR achieved by users located at a position with a polar angle of θ can be derived from (19) with the PDF transformation rule as:

$$f_\gamma(\gamma|\theta) = \left.\frac{f_r(r|\theta)}{\left|\frac{\partial}{\partial r}\gamma(r, \theta)\right|}\right|_{r=\Gamma(\hat{\gamma}|\theta)}, \tag{21}$$

where $\Gamma(\hat{\gamma}|\theta)$ is the inverse function of (18) with respect to the variable r in the interval $\hat{\gamma} \in [\gamma(r_{\max}(\theta), \theta), \gamma(0, \theta)]$. Using (20) and (21), the joint PDF of γ and θ can be calculated by adopting Bayes' theorem as:

$$f_{\gamma,\theta}(\gamma, \theta) = f_\gamma(\gamma|\theta) f_\theta(\theta). \tag{22}$$

Furthermore, by integrating (22) from 0 to 2π, the PDF of γ can be derived as:

$$f_\gamma(\gamma) = \int_0^{2\pi} f_{\gamma,\theta}(\gamma, \theta)\, \mathrm{d}\theta. \tag{23}$$

Finally, the CDF of the SINR for a user can be calculated as:

$$F_\gamma(\hat{\gamma}) = \int_{\hat{\gamma}}^{\infty} f_\gamma(\gamma)\, \mathrm{d}\gamma. \tag{24}$$

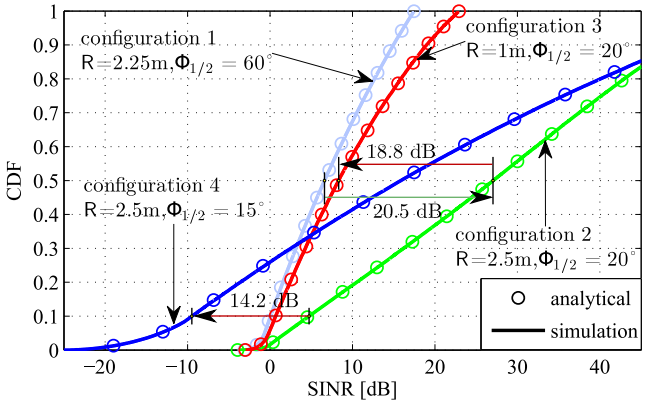

Fig. 3. Cumulative distribution function of the SINR per subcarrier with (R = 2.25 m, $\Phi_{1/2} = 60°$), (R = 2.5 m, $\Phi_{1/2} = 20°$), (R = 1 m, $\Phi_{1/2} = 20°$) and (R = 2.5 m, $\Phi_{1/2} = 15°$).

Fig. 3 shows the SINR CDF numerical results of the analytical approach for optical attocells with different configurations. The system parameters are listed in Table. I. For each optical attocell configuration, a Monte Carlo simulation of the system is also carried out. The good agreement between the Monte Carlo simulation results and the numerical results validates the accuracy of the presented analytical approach. In order to

demonstrate the effects of varying R and $\Phi_{1/2}$, systems with four specified configurations are presented.

A typical R of 2.25 m and a general Lambertian source transmitter ($\Phi_{1/2} = 60°$) are used in the configuration 1 system, which achieves a median SINR of only 6.6 dB. By adjusting R and $\Phi_{1/2}$, the median SINR achieved by a system with the configuration 2 ($R = 2.5$ m, $\Phi_{1/2} = 20°$) increases to 27.1 dB. This shows a 20.5 dB improvement relative to the configuration 1. Using configuration 2 as a baseline, configuration 3 and 4 systems are demonstrated to see the effect of changing the value of R or $\Phi_{1/2}$, respectively. For configuration 3 ($R = 1$ m, $\Phi_{1/2} = 20°$), the decrease of R causes a significant drop of 18.8 dB in median SINR relative to the configuration 2 system. In an RF cellular network, a user in the cell centre always has an overwhelmingly shorter distance to the tagged BS than the distance to any interfering BS regardless of the cell radius. However, in an optical attocell, this feature of proximity to the tagged BS for a cell centre user is not so prominent. This is because the transmission distance in an optical attocell network is determined not only by the horizontal separation between a user and a BS, but also is determined by the vertical separation h. Therefore, in the case of which h is significant relative to the horizontal separations, the users may experience interference power which is as high as the desired signal power. For configuration 4 ($R = 2.5$ m, $\Phi_{1/2} = 15°$), the further dcrease of $\Phi_{1/2}$ causes a significant drop of 14.2 dB in the guaranteed SINR (at the 10th percentile) compared to the configuration 2 system. The variable $\Phi_{1/2}$ determines m, which controls the radiation pattern of the LED, thereby controlling the optical power spatial distribution at the observed horizontal surface. For a specified R, $\Phi_{1/2}$ should be carefully adjusted in order to guarantee enough power to achieve full coverage in the cell and at the same time not to introduce too much interference in adjacent cells. In the system with configuration 4, $\Phi_{1/2} = 15°$ is too small for edge users in the optical attocell to have sufficient signal power to overcome the noise level, which causes the poor system performance.

The parameters A_{pd}, P_{opt}, κ and R_{pd} determine the effect of receiver noise only, since all of these parameters only exist in the denominator of the noise term Ω in (18). As long as practical constraints permit, these parameters should be as large as possible to minimise the effect of the receiver noise. In case the performance is limited by interference, changing these parameters shows a minor impact on the user performance. The configuration of h is complicated and it is typically determined by the indoor environment geometry and the height of the user equipment. Therefore, its impact on the user performance is outside the scope of this work, but it will be considered in future work.

IV. Average Spectral Efficiency Assessment

The wireless downlink capacity of the optical attocell network is also considered and studied in this work. A simple estimation can be conducted using the Shannon-Hartley theorem to calculate the spectral efficiency of the optical attocell network. Since the optical attocell network is based on DCO-OFDM in the downlink, the spectral efficiency can be expressed as [4]:

$$\rho(r,\theta) = \frac{K-2}{2K}\log_2\left(1+\gamma(r,\theta)\right). \tag{25}$$

Accordingly, the average spectral efficiency is calculated as:

$$\mathbb{E}[\rho] = \int_0^{2\pi}\left(\int_0^{r_{\max}(\theta)} \rho(r,\theta) f_r(r|\theta)\mathrm{d}r\right) f_{\boldsymbol{\theta}}(\theta)\mathrm{d}\theta. \tag{26}$$

The results in III-B show that the appropriate configurations of R and $\Phi_{1/2}$ are interdependent. Therefore, instead of controlling $\Phi_{1/2}$, a parameter δ, which characterises the relationship between R and $\Phi_{1/2}$, can be manipulated in order to evaluate its effects on the average spectral efficiency. The general function of δ is to achieve coarse control of the spatial distribution of the received optical power in an optical attocell. It is realised by forcing the received optical power at a specified region of the optical attocell to be half of the power that is received at the cell centre. This concept is illustrated in Fig. 4. The parameter δ is defined as a real number between 0 and 1. At the same time, α_1 and α_2 are defined as two points with $r = 0$ and $r = \delta R$, respectively. The polar angle of the point is independent of the corresponding received optical power. For a specified δ, m needs to be adjusted to fulfil the following criterion:

$$P_{\mathrm{opt}} G_{s,\alpha_1} = 2 P_{\mathrm{opt}} G_{s,\alpha_2}. \tag{27}$$

By inserting (12) in (27), m can be determined as a function of δ as follows:

$$m = 2/\log_2\left(\left(\frac{\delta R}{h}\right)^2 + 1\right) - 3. \tag{28}$$

The impact of the configuration of δ and R on the achievable average spectral efficiency is shown in Fig. 5. The relationship between the average spectral efficiency and δ for R=1 m, 1.5 m, 2 m and 2.5 m is demonstrated. The other system parameters used in this study are listed in Table. I. The results show that as δ increases from 0.2, the average spectral

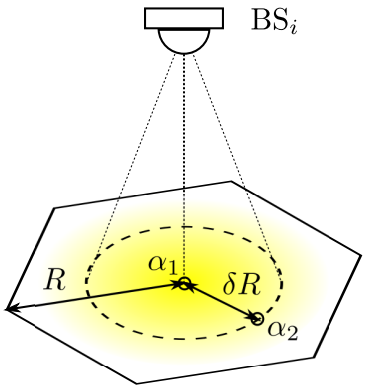

Fig. 4. α_1 is located at the pole, α_2 has a radius of δR. $\Phi_{1/2}$ is configured to make the received optical power at α_1 two times higher than the received optical power at α_2.

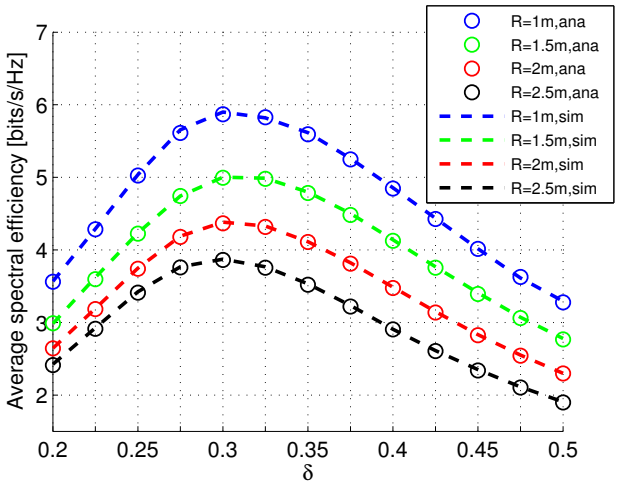

Fig. 5. Average spectral efficiency versus δ for R=1 m, 1.5 m, 2 m, 2.5 m. The notation 'ana' denotes the analytical result, while 'sim' denotes the simulated result.

efficiency also increases initially. However, when δ approaches a value of around 0.3, the average spectral efficiency reaches a peak value. With a further increase in δ, the average spectral efficiency decreases. All of the four cases for different values of R show this same trend. It is interesting to note that with a fixed δ, the average spectral efficiency of the system is higher for smaller values of R, which is a desired outcome as it favours small cell deployment. Among the demonstrated systems, the system for $R = 1$ m offers the highest average spectral efficiency of 5.9 bits/s/Hz at $\delta = 0.3$. These results indicate a general way to configure R and $\Phi_{1/2}$ with a given setting for the other parameters. This can be achieved by initially setting R to be as small as possible. Then, by finding the value of δ for which the optical attocell network achieves the highest average spectral efficiency. Fig. 5 also shows that the optimal value of δ varies little with R. Finally, based on the optimal δ, the corresponding $\Phi_{1/2}$ can be evaluated using (28).

Although the described method for optimising R and $\Phi_{1/2}$ can lead to high average spectral efficiency, there are many practical factors which further limit these parameters. For example, R cannot be too small, since this would lead to excessive handover requirements for moving users and would lead to massive optical hardware installations. Moreover, a LED with small $\Phi_{1/2}$ is undesired for illumination purposes.

V. Conclusion

This paper proposed a framework for the system-level analysis of the downlink transmission in a DCO-OFDM-based optical attocell network. An analysis for a LOS link in terms of SINR and average spectral efficiency was proposed. The impact of an optical attocell radius R and the impact of the LED half-power semi-angle were analysed in terms of achievable SINR and average spectral efficiency for a downlink transmission. The results showed that these parameters play key roles in achieving high SINR and spectral efficiency. Guidelines for the configuration of R and $\Phi_{1/2}$ to achieve high average spectral efficiency were provided. An optical attocell network achieving an average spectral efficiency of 5.9 bits/s/Hz was demonstrated. However, the impact of the variations in the vertical separation between a BS and a user and the impact of the variations in the receiver orientation were not considered in this study. In addition, the effects of shadowing and link blockage were omitted. These issues will be considered in future work.

Acknowledgement

Professor Haas acknowledges support from the Engineering and Physical Sciences Research Council (EPSRC) under Established Career Fellowship grant EP/K008757/1.

References

[1] H. Elgala, R. Mesleh, and H. Haas, "Indoor Optical Wireless Communication: Potential and State-of-the-Art," *IEEE Commun. Mag.*, vol. 49, no. 9, pp. 56–62, Sep. 2011, ISSN: 0163-6804.

[2] A. Jovicic, J. Li, and T. Richardson, "Visible Light Communication: Opportunities, Challenges and the Path to Market," *IEEE Commun. Mag.*, vol. 51, pp. 26–32, Dec. 2013.

[3] M. Alouini and A. Goldsmith, "Area Spectral Efficiency of Cellular Mobile Radio Systems," *IEEE Trans. Veh. Technol.*, vol. 48, no. 4, pp. 1047–1066, Jul. 1999.

[4] S. Dimitrov and H. Haas, "Information Rate of OFDM-Based Optical Wireless Communication Systems with Nonlinear Distortion," *J. Lightw. Technol.*, vol. 31, no. 6, pp. 918–929, Mar. 15 2013.

[5] D. Tsonev, S. Sinanovic, and H. Haas, "Complete Modeling of Nonlinear Distortion in OFDM-based Optical Wireless Communication," *J. Lightw. Technol.*, vol. 31, no. 18, pp. 3064–3076, Sep. 15 2013.

[6] H. Haas, "High-speed wireless networking using visible light," SPIE Newsroom, Apr.19 2013.

[7] D. Tsonev and H. Haas, "Avoiding Spectral Efficiency Loss in Unipolar OFDM for Optical Wireless Communication," in *Proc. of the Int. Conf. on Commun. (ICC)*, Sydney Australia, Jun. 10–14 2014.

[8] G. W. Marsh and J. M. Kahn, "Channel Reuse Strategies for Indoor Infrared Wireless Communications," *IEEE Trans. Commun.*, vol. 45, no. 10, pp. 1280–1290, Oct. 1997.

[9] D. O'Brien and M. Katz, "Optical Wireless Communications within Fourth-Generation Wireless Systems [Invited]," *J. Opt. Netw.*, vol. 4, no. 6, pp. 312–322, Jun. 2005.

[10] D. Wu, Z. Ghassemlooy, H. Le-Minh, S. Rajbhandari, and Y. Kavian, "Power Distribution and Q-factor Analysis of Diffuse Cellular Indoor Visible Light Communication Systems," in *16th Eur. Conf. Netw. and Opt. Commun. (NOC 2011)*, Newcastle upon Tyne, UK, 20–22 Jul. 2011, pp. 28–31.

[11] J. Gozalvez, "Heterogeneous Wireless Networks [Mobile Radio]," *IEEE Veh. Technol. Mag.*, vol. 6, no. 2, pp. 9–13, Jun. 2011.

[12] J. Grubor, S. Randel, K.-D. Langer, and J. Walewski, "Bandwidth-efficient Indoor Optical Wireless Communications with White Light-Emitting Diodes," in *6th International Symposium on Communication Systems, Networks and Digital Signal Processing*, Graz, Jul., 25 2008, pp. 165–169.

[13] J. M. Kahn and J. R. Barry, "Wireless Infrared Communications," *Proc. IEEE*, vol. 85, no. 2, pp. 265–298, Feb. 1997.

[14] H. Elgala, R. Mesleh, and H. Haas, "Practical Considerations for Indoor Wireless Optical System Implementation Using OFDM," in *Proc. IEEE 10th Int. Conf. Telecommun. (ConTel)*, Zagreb, Croatia, Jun. 8–10 2009, pp. 25–29.

[15] J. Armstrong and B. J. C. Schmidt, "Comparison of Asymmetrically Clipped Optical OFDM and DC-Biased Optical OFDM in AWGN," *IEEE Commun. Lett.*, vol. 12, no. 5, pp. 343–345, May 2008.

[16] D. Stoyan, W. S. Kendall, and J. Mecke, *Stochastic Geometry and its Applications*, 2nd ed. John Wiley and Sons, 1995.